OPEN ACCESS
CellPress

Cell Reports
Article

Alternative 3′ UTR Selection Controls PAR-5 Homeostasis and Cell Polarity in *C. elegans* Embryos

Martin Mikl[1,*] and Carrie R. Cowan[1,*]
[1]Research Institute of Molecular Pathology (IMP), 1030 Vienna, Austria
*Correspondence: mmikl@gmx.at (M.M.), cowan@imp.ac.at (C.R.C.)
http://dx.doi.org/10.1016/j.celrep.2014.08.004

SUMMARY

Cell polarity in one-cell *C. elegans* embryos guides asymmetric cell division and cell-fate specification. Shortly after fertilization, embryos establish two antagonistic cortical domains of PAR proteins. Here, we find that the conserved polarity factor PAR-5 regulates PAR domain size in a dose-dependent manner. Using quantitative imaging and controlled genetic manipulation, we find that PAR-5 protein levels reflect the cumulative output of three mRNA isoforms with different translational efficiencies mediated by their 3′ UTRs. 3′ UTR selection is regulated, influencing PAR-5 protein abundance. Alternative splicing underlies the selection of *par-5* 3′ UTR isoforms. 3′ UTR splicing is enhanced by the SR protein kinase SPK-1, and accordingly, SPK-1 is required for wild-type PAR-5 levels and PAR domain size. Precise regulation of *par-5* isoform selection is essential for polarization when the posterior PAR network is compromised. Together, strict control of PAR-5 protein levels and feedback from polarity to *par-5* 3′ UTR selection confer robustness to embryo polarization.

INTRODUCTION

In *C. elegans* embryos, cell fate is established through a series of asymmetric cell divisions. These divisions rely on reciprocal domains of PAR proteins at the cell cortex. The PAR proteins were originally found as *par*titioning-defective mutants in a screen that directly assayed cell fate in early embryos (Kemphues et al., 1988). Immediately after fertilization, the *C. elegans* embryo is unpolarized, and the anterior PAR protein (aPAR) complex—consisting of the PDZ domain containing proteins PAR-3 and PAR-6 and the serine/threonine kinase PKC-3—is distributed uniformly over the cortex. Cell polarization is initiated about 20 min after fertilization, when a signal from the centrosome triggers local downregulation of the acto-myosin cortex, breaking cortical symmetry. The break triggers a large-scale movement of the contractile acto-myosin cortex, which in turn generates cortical flows that move the aPARs away from the symmetry breaking site (Goehring et al., 2011; Munro et al., 2004). Removal of aPARs from this region allows the posterior PAR proteins (pPARs)—the RING domain protein PAR-2 and subsequently the MARK family serine/threonine kinase PAR-1—to localize to the cortex, forming two antagonistic cortical domains and defining the anterior-posterior axis. In addition to these essential *par* genes, enhancer and suppressor screens identified molecules that contribute to polarization but are only necessary in a compromised background (Fievet et al., 2013; Labbé et al., 2006; Morton et al., 2012). Further genetic analyses showed that parallel pathways or backup mechanisms ensure robustness of polarity establishment when the system is perturbed (Beatty et al., 2010, 2013; Hoege et al., 2010; Motegi et al., 2011).

Robustness in development, or canalization, was defined by Waddington (1942) as the consistency of a phenotype despite the genetic diversity that must necessarily exist in a population. Cell polarization in *C. elegans* embryos is robust, refractive to numerous genetic perturbations, and accommodating stochastic variation. For instance, PAR domain size shows little variation among embryos, even when the general pace of development is accelerated or slowed down (unpublished data). Upon entry into mitosis (marked by nuclear envelope breakdown; NEBD) in the first cell cycle, the aPAR and pPAR cortical domains extend to 55% and 45% embryo length, respectively. PAR domain size has a direct effect on cell-fate decisions because the PAR proteins directly control the distribution of cell-fate determinants. How is PAR domain size precisely controlled in wild-type embryos?

Despite the robustness of polarization, overexpression or partial depletion of aPARs or pPARs can influence the size of the cortical PAR domains in otherwise wild-type embryos (Goehring et al., 2011). Goehring et al. (2011) suggest that the amount of pPARs limits the size of the posterior domain. Furthermore, redundancy and feedback loops can buffer polarity against imbalances in aPAR/pPAR levels (Motegi and Seydoux, 2013). For example, a weak *par-2* mutant is synthetically lethal with depletion of the tumor suppressor LGL-1 (Beatty et al., 2010; Hoege et al., 2010). *lgl-1(−)* mutants upregulate PAR-6 (Beatty et al., 2013), suggesting an aPAR/pPAR imbalance. Conversely, overexpression of LGL-1 can rescue severe loss of PAR-2, indicating that LGL-1 can function for PAR-2 (Beatty et al., 2010; Hoege et al., 2010). It remains unknown how PAR protein levels are tightly controlled to achieve the reproducible domain sizes observed in wild-type embryos. In general, control of protein homeostasis in one-cell *C. elegans* embryos is not understood, despite increasing evidence that protein levels can dictate function in a dose-dependent manner (Decker et al., 2011; Goehring and Hyman, 2012; Greenan et al., 2010). Changes in domain size

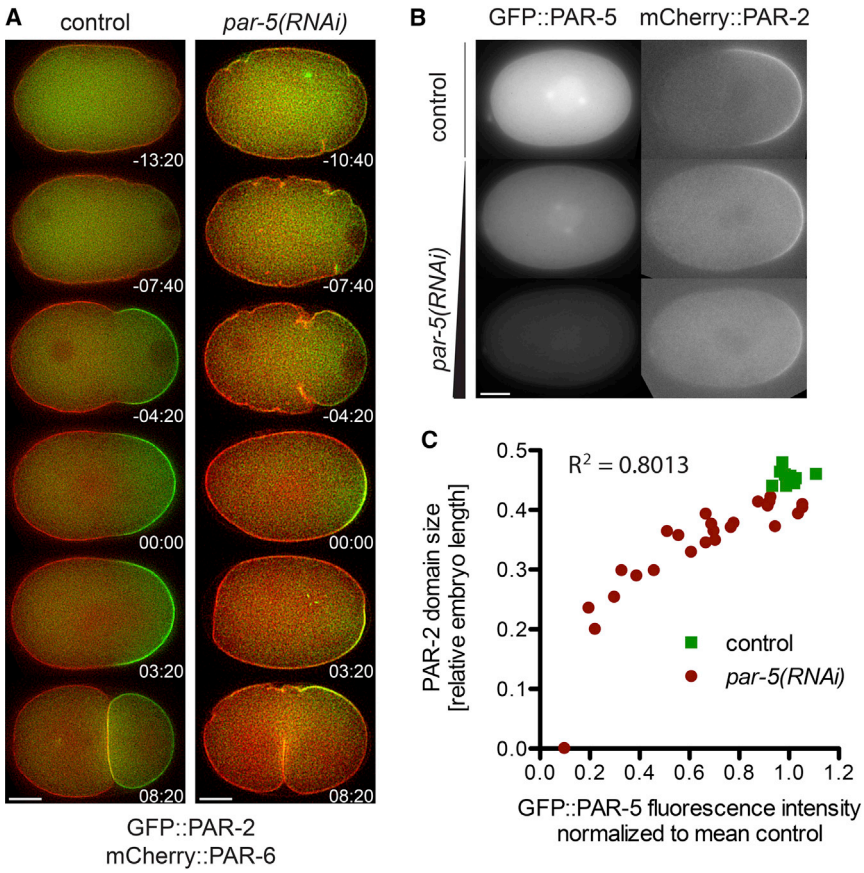

Figure 1. PAR-5 Levels Correlate with PAR Domain Size

(A) Time-lapse images of PAR polarity establishment in one-cell *C. elegans* embryos. Deconvolved images of control (left) and *par-5(RNAi)* embryos (right) expressing GFP::PAR-2 and mCherry::PAR-6 are shown. Times (min:s) relative to NEBD are shown. Posterior is to the right. Scale bars, 10 μm.

(B) Control and partial PAR-5-depleted embryos expressing GFP::PAR-5 and mCherry::PAR-2 at NEBD. Scale bar, 10 μm.

(C) PAR-2 domain size relative to integrated GFP::PAR-5 fluorescence intensity in individual embryos.

See also Figure S1 and Movies S1, S2, S3, and S4.

upon increasing or decreasing PAR-2 or PAR-6 levels are more modest than the changes in total protein would predict (Goehring et al., 2011). A decrease in PAR-6 by 40% or an increase by 25% still leads to normal-sized PAR domains (Beatty et al., 2013; Pacquelet et al., 2008). The amounts of cortical PAR proteins influence the size of the domains, but this cannot account for the precise regulation of PAR domain size in the embryo. What other processes ensure precise and robust polarization?

Here, we find that robust PAR domain size control requires the ubiquitous PAR protein PAR-5. PAR-5 protein levels correlate directly with PAR-2 domain size. PAR-5 protein levels appear to be controlled by a gene regulatory mechanism involving alternative 3′ UTR splicing of the *par-5* mRNA, mediated by the SR protein kinase SPK-1. *par-5* mRNA isoform selection was essential for cell polarity establishment in compromised backgrounds, including a weak *par-2* mutant. In addition, *par-5* mRNA isoform selection changed in response to perturbations in cell polarity, suggesting that splicing of *par-5* mRNA may react to variability in the polarization system and thus ensure robustness.

RESULTS

PAR-5 Is a Dose-Dependent Regulator of PAR Domain Size

To identify molecules regulating PAR domain size, we performed an RNAi-based loss-of-function screen of ~110 genes selected for their known involvement in early embryogenesis (Table S1; Sönnichsen et al., 2005). Each gene was tested for its effect on posterior domain formation by time-lapse microscopy of embryos expressing GFP::PAR-2 following depletion by RNAi. We identified 17 genes leading to smaller and 5 genes leading to larger PAR-2 domains. Three genes resulting in smaller PAR-2 domains act in actomyosin contractility and are known to affect posterior domain size (C56G7.1, F11H8.4, and F20G4.3; Motegi et al., 2011; Zonies et al., 2010). One of the candidates necessary for normal posterior domain size was *par-5* (M117.2), a gene encoding a 14-3-3 protein already known to be required for correct cell polarity in early *C. elegans* embryos (Morton et al., 2002). PAR-5 depletion led to smaller PAR-2 domains of variable size and a loss of mutual exclusion of aPARs and pPARs (Figure 1A). *par-5(RNAi)* embryos often failed to maintain the PAR-2 domain through mitosis and divided symmetrically. Notably, the characteristic defects changed with the strength of the depletion, from a specific reduction in the size of the posterior domain ("mild" phenotype) with nonoverlapping cortical PAR domains to an undetectable posterior domain due to complete overlap of aPARs and pPARs ("strong" phenotype, Figure S1; Movies S1, S2, S3, and S4). Embryos with a strong loss of PAR-5 phenotype also showed contractility defects.

To understand the phenotypic variation in *par-5(RNAi)* embryos, we assessed whether PAR-2 domain size correlated with differences in PAR-5 protein levels. We generated a GFP::PAR-5 transgene under the control of endogenous *par-5* regulatory elements (+1 kb promoter and 3′ UTR) and inserted this into a defined ectopic locus (Experimental Procedures). We used integrated GFP fluorescence intensity to approximate PAR-5 protein levels at NEBD. GFP::PAR-5 showed uniform cytoplasmic distribution in early embryos with an enrichment at the cell cortex (Figure S2B; Morton et al., 2002). Among wild-type embryos, the SD of GFP::PAR-5 levels was less than 5% (n = 9), suggesting that PAR-5 may be tightly regulated. PAR-2 domain size exhibited a similarly small amount of variation

(SD 3%; n = 9). Following PAR-5 depletion, we found that the amount of GFP::PAR-5 correlated linearly with the size of the PAR-2 domain at NEBD (R^2 = 0.80; Figures 1B and 1C). Reductions in PAR-5 that were at our limit of detection nonetheless had quantifiable effects on PAR-2 domain size, indicating that domain size is highly sensitive to PAR-5 levels. These results indicate that PAR-5 helps set PAR-2 domain size in a dose-dependent manner. Thus, regulation of PAR-5 levels is critical to controlling domain size.

par-5 3′ UTR Isoform Ratios Are Regulated

How are PAR-5 protein levels precisely regulated? *par-5* mRNA is provided maternally, and thus control over PAR-5 protein abundance likely occurs posttranscriptionally. PAR-5 protein levels in the early embryo were similar to those in the gonad and oocytes based on GFP::PAR-5 fluorescence (Figure S1C), suggesting that PAR-5 is synthesized in the gonad and contributed maternally to early embryos. Using 3′ rapid amplification of cDNA ends (RACE) and quantitative PCR (qPCR), we confirmed earlier findings by Wang and Shakes (1997) that the *par-5* locus makes three mRNA isoforms that share the same coding sequence but contain alternative 3′ UTRs (Figure 2A). In mRNA isolated from whole worms, the short isoform *par-5::utr.3* is most abundant, whereas the long isoforms *par-5::utr.1* and *par-5::utr.2* together make up approximately 20% of total *par-5* mRNA (Figure 2B).

par-5 mRNA isoform selection seemed constant in worms of the same stage but varied considerably during development: total *par-5* mRNA abundance decreased during embryogenesis, but the relative amounts of *par-5::utr.1* and *par-5::utr.2* increased significantly, peaking at the first larval stage (Figure 2B). During postembryonic development, *par-5* mRNA isoform selection shifted progressively toward the short 3′ UTR isoform, *par-5::utr.3*, in line with the general tendency for *C. elegans* 3′ UTRs (Mangone et al., 2010). This elaborates the results of Wang and Shakes (1997), indicating that both *par-5* isoform selection and mRNA expression change during development. In addition, *par-5* isoform selection was modulated during the adaptation to growth at higher temperature (Figure 2C), which correlated with a change in PAR-5 protein (Figure 2D), whereas overall *par-5* mRNA levels remained largely constant (Figure 2C). A progressive increase in PAR-5 protein levels could also be observed during embryogenesis (Figures 2E and 2F), coincident with an increased contribution of *par-5::utr.2*.

par-5::utr.2 results from a splicing event in the 3′ UTR, downstream of the "stop" codon and thus should be targeted by nonsense mediated decay (NMD). NMD-deficient worms, however, showed no differences in *par-5* mRNA isoform abundance or changes in PAR-5 protein levels attributable to NMD, suggesting that *par-5* isoforms are not degraded by NMD (Figures S3A and S3B). Instead, *par-5* isoform selection appears to be regulated and might be used to control protein levels.

par-5 3′ UTR Isoforms Have Different Translational Efficiencies

3′ UTRs regulate protein expression in the *C. elegans* germline (Merritt et al., 2008). To determine if *par-5*'s alternative 3′ UTRs might control PAR-5 protein levels, we aimed to assess the individual contributions of each *par-5* mRNA isoform to PAR-5 protein. Because the *utr.3* sequence entirely overlaps with *utr.1*, and the *utr.2* sequence overlaps entirely with *utr.1*, we could only design RNAi constructs targeting all three isoforms or both *utr.1* and *utr.2*. Given these limitations, we could not assess the contributions of the individual isoforms by selective depletion.

Instead, we investigated each *par-5* isoform for its translational efficiency. We generated GFP::PAR-5 transgenes controlled specifically by *utr.1*, *utr.2*, or *utr.3*. As for wild-type GFP::PAR-5, we used the endogenous promoter region and inserted a single copy of the transgene into the same ectopic locus (Figure S3C; Experimental Procedures). To generate the specific 3′ UTRs, we manipulated the splice junctions that are required to generate *par-5::utr.2* and the proximal poly(A) site required for *par-5::utr.3*. The splice junctions in the 3′ UTR of *par-5* differ from splicing consensus sequences, mainly at the 5′ splice site (Figure 3A). We mutated the 5′ and 3′ splice sites to perfectly match the consensus sequences (Figure 3B), which led to the predominant usage of these splice sites and production of *par-5::utr.2* almost exclusively (Figure 3C), similar to a construct with prespliced *par-5* 3′ UTR, whose DNA sequence did not contain the 3′ UTR introns. Conversely, we mutated the splice junctions by flipping the GT and AG dinucleotides at the 5′ and 3′ end of the introns, respectively, leading to retention of these introns and thus the production of only *par-5::utr.1* and *par-5::utr.3*. Additionally, mutating the proximal poly(A) site led to the exclusive production of the long unspliced *par-5::utr.1*. Finally, we removed the distal poly(A) sites to force production of only the short *par-5::utr.3*. By changing *par-5*'s downstream sequence, we could predictably control *par-5* 3′ UTR selection (Figures 3C, S3D, and S3E; Experimental Procedures).

To test the three *par-5* mRNA isoforms for translational efficiency, we took GFP fluorescence intensity in early embryos as a measure of PAR-5 expression and standardized this to the abundance of the respective *gfp::par-5::utr* mRNA. The three *par-5* isoforms produced different amounts of PAR-5 in one-cell embryos (Figure 3D), with *utr.1* and *utr.2* producing the most protein per mRNA, approximately 3- and 2-fold more than *utr.3*, respectively (Figure 3E). We did not observe different localization or expression patterns of the isoforms (data not shown), arguing against 3′ UTR-dependent spatial or temporal control. Thus, the long *par-5* 3′ UTRs, *utr.1* and *utr.2*, promote more translation than the short *par-5* 3′ UTR, *utr.3*, in early embryos. However, *par-5::utr.1* did not contribute markedly to PAR-5 protein when other mRNA isoforms could be generated from the same locus because targeting *par-5::utr.1* (and *par-5::utr.2*) in a strain expressing GFP::PAR-5 under the control of *par-5::utr.1/3* did not reduce GFP::PAR-5 levels in one-cell embryos (Figure S3E; Experimental Procedures). *par-5::utr.1* mRNA may not be present at this particular stage or may contribute negligibly to PAR-5 protein. Selection between *utr.2* and *utr.3* therefore seems decisive in controlling PAR-5 levels. The choice between *utr.2* and *utr.3* is mediated by one event: splicing out of the first 3′ UTR intron to remove the proximal poly(A) site needed to generate *utr.3*.

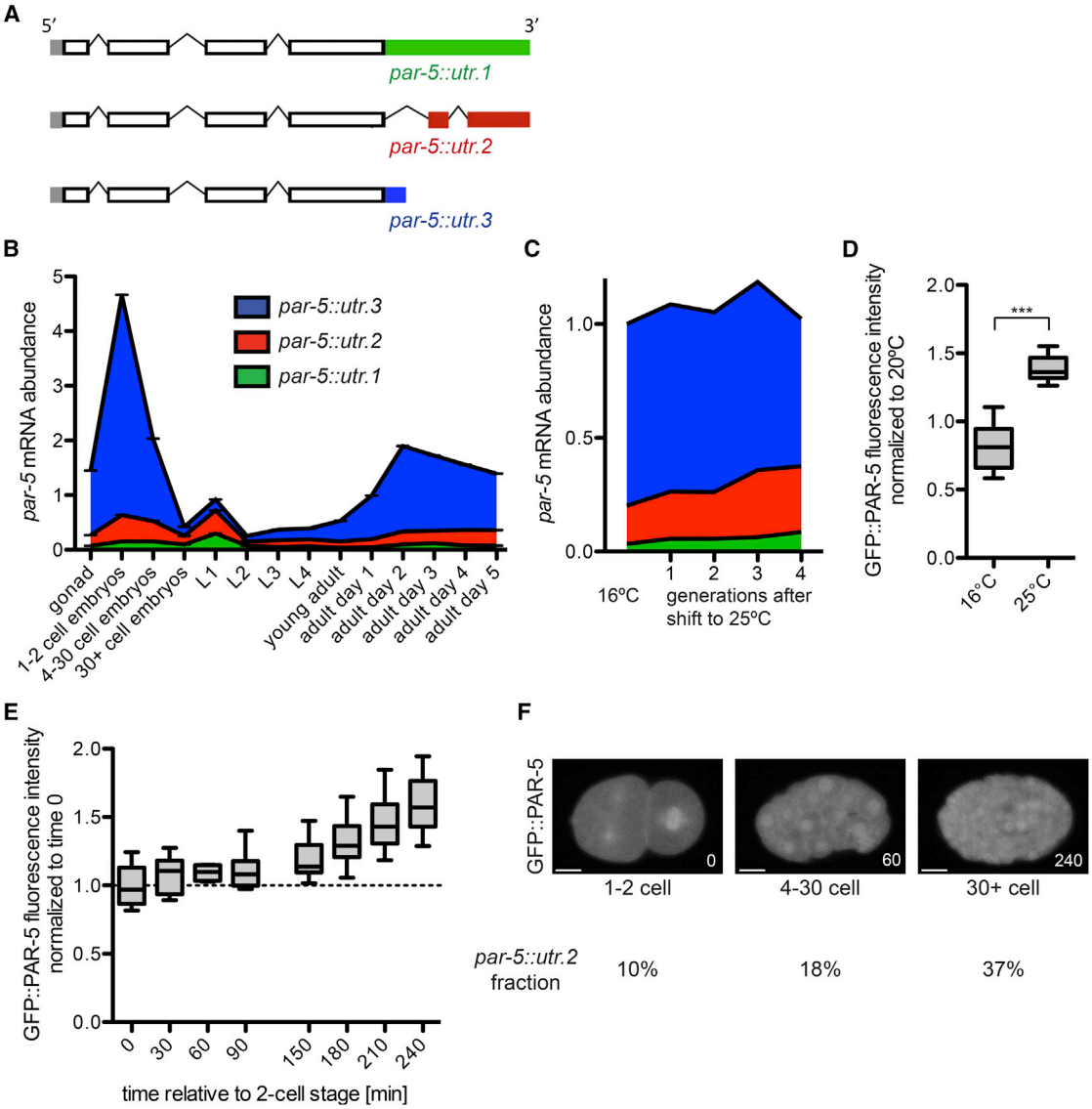

Figure 2. *par-5* 3′ UTR Isoform Selection Is Regulated

(A) Model of *par-5* mRNA isoforms.

(B) Cumulative isoform contributions at different developmental stages as determined by qPCR and normalized to *ctb-1* and *act-1* (green, *par-5::utr.1*; red, *par-5::utr.2*; blue, *par-5::utr.3*; n = 2–7 biological replicates).

(C) Cumulative isoform contributions during adaptation to growth at 25°C as determined by qPCR and normalized to *ctb-1* and *act-1* (green, *par-5::utr.1*; red, *par-5::utr.2*; blue, *par-5::utr.3*; n = 3–5 biological replicates).

(D) GFP::PAR-5 levels are increased in embryos grown at 25°C. Whiskers indicate 10th–90th percentile ranges. Asterisks indicate statistically significant changes (two-tailed t test, ***$p < 0.001$; n = 37 and 17 embryos).

(E) Integrated fluorescence intensity of GFP::PAR-5 at different stages of embryogenesis, normalized to the mean value at time 0 (n = 4–12 embryos). Whiskers indicate 10th–90th percentile ranges.

(F) Confocal images of an embryo expressing GFP::PAR-5 at different stages of embryogenesis. Times (min) are relative to two-cell stage. Scale bars, 10 μm.

SPK-1 Is Required for Efficient *par-5* 3′ UTR Splicing, Wild-Type PAR-5 Protein Levels, and Correct Cell Polarity

In order to understand how *par-5* isoform selection regulates PAR-5 protein levels and polarity establishment, we identified molecules controlling *par-5* 3′ UTR splicing. Alternative splicing in *C. elegans*, as in other eukaryotes, is regulated in part by a semiredundant family of SR proteins and the SR protein kinase SPK-1 (Kuroyanagi et al., 2000). We tested a subset of these genes by RNAi for an effect on *par-5* isoform selection, selecting genes required for embryogenesis. From the candidates tested, only *spk-1(RNAi)* worms showed a reproducible reduction specifically in *par-5::utr.2*, the isoform with the long, spliced 3′ UTR (Figures 4A and 4B). *spk-1* mRNA levels following partial

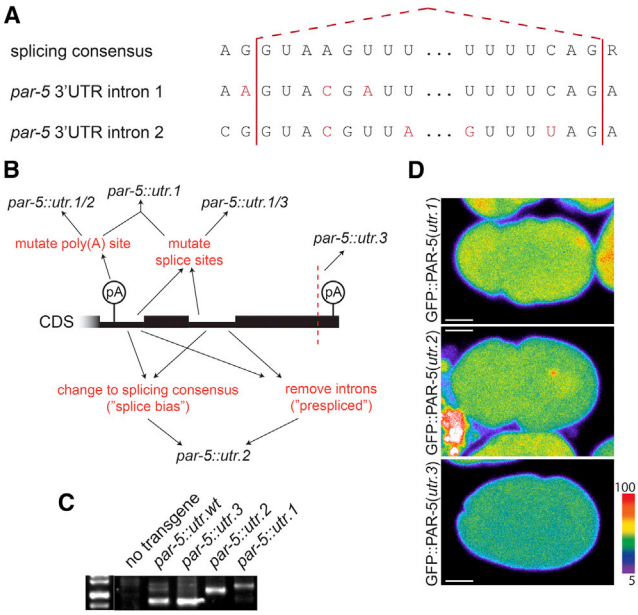

Figure 3. *par-5* 3′ UTR Isoforms Have Different Translational Efficiencies

(A) Splice site sequences in the *par-5* 3′ UTR. Deviations from the splicing consensus are indicated in red.

(B) Strategy for generating *par-5* isoform-specific transgenes.

(C) 3′ RACE of ectopic *par-5* constructs carrying mutations in splice and poly(A) sites.

(D) Pseudocolored images of one-cell embryos (at approximately the same developmental stage) expressing GFP::PAR-5 under the control of *par-5::utr1*, *par-5::utr.2*, or *par-5::utr.3*. Purple indicates low and red high signal intensity. Scale bars, 10 μm.

(E) Integrated fluorescence intensities of GFP::PAR-5 under the control of isoform-specific 3′ UTRs normalized to GFP::PAR-5 (*utr.wt*) and adjusted for abundance of the respective *gfp::par-5::utr* mRNA. Whiskers indicate 10th–90th percentile ranges. ANOVA showed significant ($p < 0.0001$) differences between the groups. Bonferroni's multiple comparison test showed highly significant ($p < 0.001$) differences for all combinations (n = 88, 29, and 28 embryos).

See also Figure S3.

depletion correlated with the level of *par-5::utr.2* in individual biological replicates ($R^2 = 0.76$; Figure 4C), suggesting a functional link between SPK-1 and *par-5* 3′ UTR splicing. The same effect was seen in mRNA isolated from gonads, but not from gonadless animals (Figure 4D), indicating that SPK-1's role in *par-5::utr.2* splicing is specific to the germline. Thus, the splicing regulator SPK-1 helps determine *par-5* 3′ UTR selection.

To test if reduced *par-5::utr.2* splicing in SPK-1-depleted worms reflected a global splicing defect, we performed Illumina sequencing of mRNA from control and *spk-1(RNAi)* worms and compared the transcriptomes of the two conditions. Overall, transcript abundances correlated well, so splicing did not appear to be generally compromised in *spk-1(RNAi)* worms. To identify genes that were affected by SPK-1 depletion, we found differences in exon expression using the DEXSeq package. We also compared the number of reads spanning a given splice junction. Combining these 2 strategies and restricting candidates to those present in all 4 biological replicates yielded a list of 26 genes whose splicing requires SPK-1 (Figure S4A). This transcriptome-wide approach confirmed the reduction in *par-5::utr.2* (Figures S4B–S4D). As for *par-5::utr.2*, many of the splicing events dependent on SPK-1 involved sequences with nonoptimal splice sites. This was most evident at the 5′ splice site, especially at the fourth and sixth nucleotides downstream of the splice site, which are preferentially uracils genome wide but were random nucleotides in SPK-1 targets (Figure S4E). Indeed, our splice site-optimized *gfp*::*par-5::utr.2* transgene did not depend on SPK-1 for splicing (Figure 4E). Thus, SPK-1, at the depletion level used, is essential for a small number of alternative splicing events, including splicing of the *par-5* 3′ UTR to generate the translationally active isoform *par-5::utr.2*.

Our results thus far suggested that SPK-1 controls *par-5* 3′ UTR alternative splicing and thereby isoform selection. Furthermore, *par-5* isoform selection may control PAR-5 protein levels through different rates of translation. We therefore wanted to test the effects of SPK-1 depletion on PAR-5 protein levels. GFP::PAR-5 levels in *spk-1(RNAi)* embryos were reproducibly decreased to approximately 81% of wild-type levels (Figures 4F and 4G). The contribution of SPK-1 was eliminated when GFP::PAR-5 was controlled by a mutated *utr.2* containing optimal splice sites or by a "prespliced" *utr.2* (Figure 4G). Thus, SPK-1 enhances splicing of the *par-5* 3′ UTR and ensures wild-type PAR-5 protein levels. We had identified SPK-1 in our initial screen for PAR-2 domain size defects (Table S1), prompting us to look again at polarity in *spk-1(RNAi)* embryos. The polarity defects of *spk-1(RNAi)* embryos resembled those of mild PAR-5 depletion, including slower expansion and smaller size of the PAR-2 domain (Figures 5A–5C). Therefore, disrupting *par-5* 3′ UTR selection by interfering with SPK-1-dependent splicing decreases the fidelity of polarity establishment, similar to depletion of PAR-5.

par-5 Isoform Selection Contributes to the Robustness of Cell Polarity

Given that SPK-1 depletion had a very specific effect on *par-5* isoform selection, i.e., reduction of *par-5::utr.2* by half, we wanted to determine if depletion of *par-5::utr.2* alone would have a similar effect on PAR-5 abundance and polarity establishment or if *par-5::utr.3* alone is sufficient to ensure robust polarization. We found that depletion of *par-5::utr.2* reduced PAR-5 by 20%, similar to the 19% reduction we saw in *spk-1(RNAi)* embryos (Figure 6A). *par-5::utr.2(RNAi)* embryos, however, showed a very mild defect in PAR-2 domain size and were viable (Figures 6B and 6C), suggesting that SPK-1 depletion affects additional processes important for cell polarization.

The more severe polarity defects in *spk-1(RNAi)* embryos compared to *par-5::utr.2(RNAi)* embryos may arise from additive mis-regulation in SPK-1-depleted embryos. Other SPK-1 targets

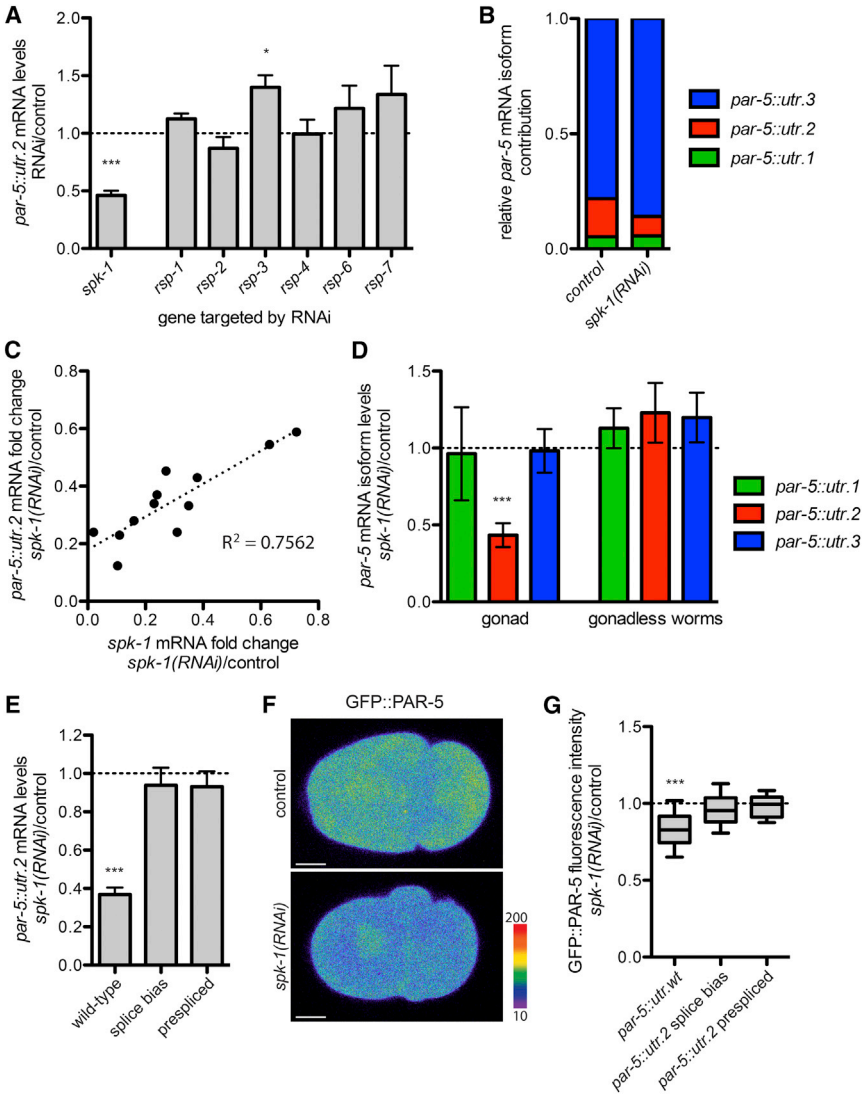

Figure 4. Depletion of SPK-1 Affects *par-5* 3′ UTR Splicing and Reduces PAR-5 Protein Levels

(A) Fold change of *par-5::utr.2* in RNAi compared to control worms. Error bars denote SEM. Asterisks indicate statistically significant changes to control (two-tailed t test, *p < 0.5, ***p < 0.001; n ≥ 2 biological replicates).

(B) *par-5* mRNA isoform contributions to total *par-5* mRNA in control and *spk-1(RNAi)* worms.

(C) Fold change of *par-5::utr.2* in *spk-1(RNAi)* worms compared to control worms plotted against the reduction in *spk-1* mRNA in individual RNA isolations.

(D) Fold change of *par-5* isoforms in wild-type gonads or gonadless worms (*pgl-1(bn101)*) in *spk-1(RNAi)* compared to control. Error bars denote SEM. Asterisks indicate statistically significant changes to control (two-tailed t test, ***p < 0.001; n ≥ 3 biological replicates).

(E) Fold change of *par-5::utr.2* made from wild-type, splice biased, or prespliced 3′ UTR in *spk-1(RNAi)* compared to control (n ≥ 4 biological replicates).

(F) Pseudocolored images of one-cell embryos (at approximately the same developmental stage) expressing GFP::PAR-5 in control and *spk-1(RNAi)*. Purple indicates low and red high signal intensity. Scale bars, 10 μm.

(G) Integrated fluorescence intensity of GFP::PAR-5 under the control of *utr.wt*, splice biased *utr.2*, or prespliced *utr.2* in one-cell *spk-1(RNAi)* embryos compared to control. Whiskers indicate 10th–90th percentile ranges. Error bars denote SEM. Asterisks indicate statistically significant changes to the control condition (two-tailed t test, ***p < 0.001; n = 326, 103, and 37 embryos).

See also Figure S4.

that contribute to the polarity defect in *spk-1(RNAi)* embryos might be directly involved in cell polarity or might be factors that generally compromise development, making the embryos sensitive to small changes in PAR-5 levels. We attempted to mimic the *spk-1(RNAi)* situation by depleting *par-5::utr.2* from a number of viable mutants. We chose mutants in putative targets of SPK-1 identified by our transcriptome analysis (Figure S4A). In addition, we tested viable mutants in the polarity pathway. To assess the specificity of putative synthetic interactions, we tested mutants in general growth and metabolic pathways, including mammalian target of rapamycin and insulin signaling pathways. First, we assessed embryonic viability in mutant worms depleted of *par-5::utr.2* (Figure 6B). The weak *par-2(or640)* mutant was highly sensitive to *par-5::utr.2* depletion, with a drop in embryo viability from 90% to 5%. The PAR polarity mutants *pig-1* and *ect-2* also showed synthetic interactions with *par-5::utr.2(RNAi)*. There was little effect of *par-5::utr.2* depletion on mutants in other aspects of cell polarity establishment, growth control, or metabolism. Because of the strong synthetic interaction between *par-5::utr.2(RNAi)* and *par-2(or640)*, we next tested if cell polarity was compromised in these embryos by assessing cortical PAR-2 and PAR-3 domain size in fixed one- and two-cell embryos (Figure 6C). The *par-2(or640)* mutant—under control conditions at the permissive temperature—established and maintained normal-sized anterior and posterior PAR domains, despite a 25% reduction in PAR-2 levels (Figure S4H). Depletion of *par-5::utr.2* in *par-2(or640)* embryos led to a persistent loss of polarity: PAR-3 occupied the entire cortex in both one- and two-cell embryos. Reducing PAR-5 protein to a similar extent by depleting all *par-5* mRNA isoforms (*par-5mismatch(RNAi)*; Figure 6A) did not severely affect embryonic viability (70% viability compared to 6% in *par-5::utr.2(RNAi)*) or polarity in the *par-2(or640)* background (Figure 6C). The longer, more translationally active isoform *par-5::utr.2* thus appears to be essential when the pPAR domain is slightly compromised.

Our results suggest that PAR-5 levels determine pPAR domain size and thus ensure accurate cell polarization. A precise mixture of *par-5* mRNA isoforms with different translational efficiencies

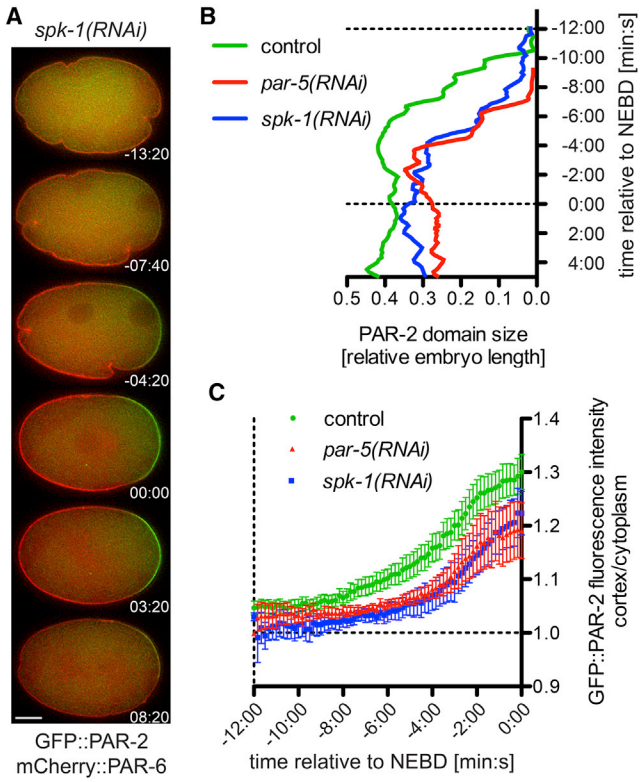

Figure 5. *spk-1(RNAi)* Embryos Exhibit Polarity Defects Reminiscent of Partial PAR-5 Depletion

(A) Deconvolved images of *spk-1(RNAi)* embryos expressing GFP::PAR-2 and mCherry::PAR-6 from time-lapse recordings. Times (min:s) are relative to NEBD. Posterior is to the right. Scale bar, 10 μm.

(B) PAR-2 domain size in control, *spk-1(RNAi)*, and *par-5(RNAi)* embryos (n = 6, 12, and 6 embryos).

(C) Accumulation of GFP::PAR-2 at the posterior cortex from symmetry breaking (−12:00) to NEBD (0:00) in control, *spk-1(RNAi)*, and *par-5(RNAi)* embryos as determined by the ratio of cortical versus cytoplasmic GFP::PAR-2 fluorescence intensity (n = 8, 7, and 6 embryos).

See also Figure S7.

cumulatively provides the correct amount of PAR-5 protein for the embryo. Given that *par-5* 3′ UTR usage appears regulated and tightly controlled (Figure 2), we asked if *par-5* mRNA isoform ratios adjust according to changing needs for PAR-5. The sensitivity of *par-2(or640)* embryos to depletion of the efficiently translated *par-5::utr.2* isoform suggested that embryos with defects in PAR polarity might require more PAR-5. We tested if PAR polarity defects influence *par-5* 3′ UTR splicing using qPCR to quantify *par-5* isoforms in *par-2(or640)* mutants. The long, translationally more active isoforms, *par-5::utr.1* and *par-5::utr.2*, were higher in *par-2(or640)* worms compared to control or other mutant worms grown under the same conditions (Figure 6D). *par-5::utr.2* and *par-5::utr.1* produce more protein per mRNA than the predominant *par-5::utr.3* isoform, suggesting that PAR-5 protein levels could be higher in *par-2* mutant embryos than in wild-type. This prediction could not be tested because of the different temperature dependencies of the *par-2* mutant and expression of GFP::PAR-5. Our results indicate feedback from PAR polarity to *par-5* isoform selection. The capacity to change the ratios of *par-5* mRNA isoforms may help ensure polarization when the system is compromised.

DISCUSSION

Here, we found that PAR domain size is regulated by PAR-5, a known polarity protein. PAR-5 acts in a dose-dependent way, and as such, PAR-5 levels appear to be tightly controlled to achieve accurate PAR polarity. The *par-5* locus encodes three mRNAs with different 3′ UTRs. The isoforms have different translational efficiencies. None of the three isoforms alone can sustain viability because only a construct with a wild-type 3′ UTR could complement a *par-5* mutant (*it55*; data not shown). Only *par-5::utr.2* and *par-5::utr.3* contribute measurably to total PAR-5 protein in wild-type embryos. The distinction between *utr.2* and *utr.3* requires alternative splicing: *utr.2* is generated by usage of 3′ UTR splice sites controlled by the SR protein kinase SPK-1. SPK-1 helps determine PAR domain size, in part through its effect on *par-5* splicing. Splicing of *par-5::utr.2* is essential for polarity establishment in a weak *par-2* mutant, correlating with an increase in *par-5::utr.2* relative to the other *par-5* isoforms. Thus, not only does *par-5* isoform selection contribute to the robustness of polarity establishment by controlling PAR-2 domain size, but PAR polarity feeds back to bias *par-5* 3′ UTR splicing.

Taking into account the different translational efficiencies of *par-5* mRNA isoforms, the relative contributions of *par-5::utr.2* and *par-5::utr.3* to total *par-5* mRNA reliably predict the observed PAR-5 protein levels in different conditions (Table 1). Differences in translational efficiency may be important for precise regulation on short time scales, such as during developmental decisions. Translation rates, however, may not produce dramatic effects on steady-state levels if other compensatory mechanisms, such as control of protein degradation, are active. Due to its long 3′ UTR, *par-5::utr.2* provides a larger platform for integrating signals (RNA binding proteins) and thus can react to environmental changes or developmental cues. A screen of posttranscriptional regulators revealed a requirement for MEX-5 and RNP-4 to maintain wild-type PAR-5 levels (Table S2). This effect was not isoform specific and hence could not account for the differences in translational efficiency among *par-5* mRNA isoforms.

The selection between *par-5* isoforms is controlled largely by the decision to splice the 3′ UTR, a decision regulated by SPK-1. Qualitative changes controlled by alternative splicing are well known in developmental decisions (Venables et al., 2012). Here, we find that alternative 3′ UTR splicing does not change the protein product but rather its abundance in a quantitative way. Adjustment of *par-5* mRNA isoform ratios allows for adjustment of PAR-5 protein levels according to need. For instance, in a PAR-2 partial loss-of-function mutant, *par-5::utr.2* contributes more to total *par-5* mRNA compared to wild-type worms. PAR polarity is established normally in this *par-2* mutant, but it is especially sensitive to PAR-5 concentration, suggesting a need for more PAR-5 protein in this compromised background. We observed a similar increase in *par-5::utr.2* and PAR-5 protein levels and a dependency on *par-5::utr.2* when worms were

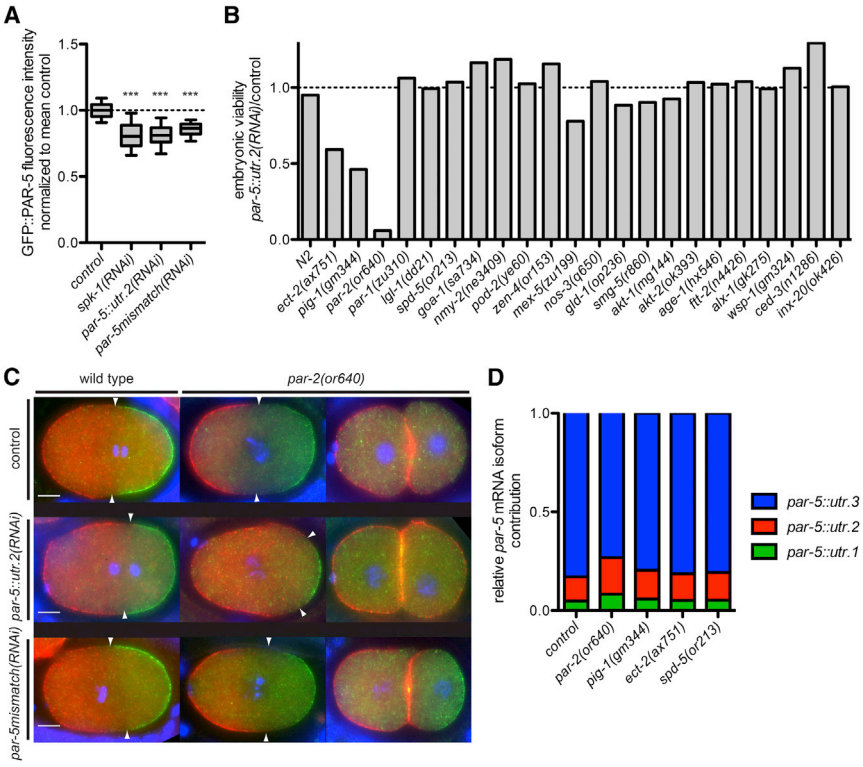

Figure 6. *par-5::utr.2* Is Required for the Robustness of Cell Polarity

(A) Integrated fluorescence intensity of GFP::PAR-5 (*utr.wt*) in one-cell embryos of control, *spk-1(RNAi)*, *par-5::utr.2(RNAi)*, and *par-5mismatch(RNAi)* (dsRNA with reduced complementarity to *par-5*) worms. Whiskers indicate 10^{th}–90^{th} percentile ranges. Asterisks indicate statistically significant changes to control (two-tailed t test, ***$p < 0.001$; n = 276, 476, 84, and 22 embryos).

(B) Effect of *par-5::utr.2(RNAi)* on embryonic viability of worm strains carrying nonlethal or conditional mutations at the permissive temperature. The ratios of percentages of hatched worms in *par-5::utr.2(RNAi)* and control are shown.

(C) Immunofluorescence images from wild-type and *par-2(or640)* embryos with or without depletion of *par-5::utr.2* or partial *par-5* depletion by *par-5mismatch(RNAi)*. Green indicates PAR-2, red indicates PAR-3, and blue indicates DNA (DAPI). Scale bars, 10 μm.

(D) *par-5* mRNA isoform contributions to total *par-5* mRNA in N2, *par-2(or640)*, *pig-1(gm344)*, *ect-2(ax751)*, and *spd-5(or213)* worms.

maintained at 25°C for multiple generations (preferred growth temperature 16°C–20°C): continuous depletion of *par-5::utr.1+2* led to polarity defects, embryonic lethality, and sterility (Figure S5; data not shown). Both in the *par-2* mutant and in worms maintained at 25°C, the increased dependency on *par-5::utr.2* (and possibly *utr.1*) could result from (1) more *par-5* mRNA depletion because more of the total *par-5* mRNA consists of the long isoforms, or (2) requirements for specific isoforms based on their translational characteristics. For instance, the switch to more efficiently translated *par-5* isoforms could be an adaptation to faster development at increased temperatures. Their considerably longer 3′ UTRs allow transacting factors to influence the rate of protein production or concentrate it spatially. In both cases, adjustments in PAR-5 levels appear to contribute robustness.

PAR-5 protein levels appear to be strictly controlled. Increased PAR-5 levels are advantageous when polarity establishment is compromised, but overexpression of PAR-5 is generally avoided. Introduction of an ectopic copy of *par-5* led to downregulation of the endogenous locus (Figure S6A). The extent of downregulation was proportional to the amount of protein made from ectopic *par-5* (Figure S6B). Depleting either endogenous or ectopic *par-5* by RNAi led to an upregulation of expression from the other *par-5* locus (Figures S6C and 6D), suggesting compensation to reach normal PAR-5 levels. The extent of compensation at the mRNA level depended on the translational efficiency of the *par-5* isoform being depleted, indicating that PAR-5 protein levels rather than mRNA molecules are monitored. Similar mechanisms might buffer against environmentally induced fluctuations in gene expression and thus contribute to the tight control of protein levels.

Not all PAR-5-dependent processes are equally sensitive to levels: in adult worms, intermediate PAR-5 depletion interferes with the DNA damage checkpoint, but only strong PAR-5 depletion disrupts cell-cycle progression and DNA stability (Aristizábal-Corrales et al., 2012). Nonetheless, tight regulation of protein levels is a general feature of PAR-5/14-3-3 proteins (Tzivion et al., 2006), and reduction as well as overexpression can be deleterious. Overexpression of 14-3-3 proteins has been linked to cancer through their role inhibiting proapoptotic pathways and controlling the cell cycle (Martin et al., 2003; Porter et al., 2006; Takihara et al., 2000). 14-3-3 protein levels are elevated in lung cancers (Nakanishi et al., 1997) and in a high percentage of colorectal carcinoma samples (Perathoner et al., 2005). Mechanisms to tightly control PAR-5 levels and prevent overexpression are therefore not only crucial for cell polarity in *C. elegans* but appear to be a general requirement of 14-3-3 proteins.

How does the precise control over PAR-5 levels relate to PAR-5's role in polarity? The molecular function of PAR-5 in cell polarity in *C. elegans* embryos is not known. Work on the *Drosophila* homolog of PAR-5, 14-3-3, has shown that phosphorylation of DmPar3/Bazooka by DmPar1 creates a binding site for DmPar5/14-3-3 (Benton and St Johnston, 2003). This binding causes the disassembly of the aPAR complex, which consequently falls off the cortex. The failure of pPARs to exclude aPARs in *C. elegans* embryos depleted of PAR-5 and the fact that we found that PAR-3 interacts with PAR-5 using immunoprecipitation followed by mass spectrometry (unpublished data) suggest a similar function in *C. elegans*. The phenotype of *par-5(RNAi)* embryos, however, is inconsistent with a model in which PAR-5 only excludes aPARs from the cortex. Our results showed that *par-5(RNAi)* and *spk-1(RNAi)* embryos have reduced cortical PAR-2 accumulation, and depletion of PAR-5

Table 1. Prediction of PAR-5 Expression Based on 3′ UTR Isoform Contributions and Translational Efficiency

		Control		*spk-1(RNAi)*	
	Translational Efficiency	Isoform Abundance	Contribution to Protein	Isoform Abundance	Contribution to Protein
par-5::utr.2	1.75	0.15	0.2625	0.07	0.1225
par-5::utr.3	0.85	0.85	0.7225	0.85	0.7225
Expected PAR-5 protein			0.985		0.845
Measured PAR-5 protein			1		0.812

The contribution of the individual isoforms to total PAR-5 protein was calculated from their translational efficiency relative to GFP::PAR-5 under the control of *par-5::utr.wt* and the relative abundance of individual mRNA isoforms. Measured PAR-5 protein levels constitute the mean of integrated fluorescence intensities in one-cell embryos expressing GFP::PAR-5. *par-5::utr.1* did not contribute measurably to PAR-5 levels in early embryos and thus is excluded from the prediction.

in a *par-3* mutant background led to a *par-2*-like spindle orientation defect, together suggesting that PAR-5 has a role in the posterior PAR domain (Figure S7). PAR-5 might directly assist PAR-2 loading onto the cortex. Alternatively, PAR-5 might act in a parallel polarization pathway, for instance, involving LGL-1. We saw no synthetic interaction between *par-5::utr-2(RNAi)* and *lgl-1(−)*, whereas we saw strong synthetic interactions between *par-5::utr-2(RNAi)* and a weak *par-2* mutant. This difference would be consistent with a role for PAR-5 in the LGL-1 pathway, which becomes essential in the weak *par-2* mutant, although we have not investigated this further. In any case, too much or too little PAR-5 appears to disrupt the balance between anterior and posterior domains.

Many aspects of polarity establishment and maintenance in *C. elegans* embryos appear to be governed by redundant pathways (Motegi and Seydoux, 2013). Backup mechanisms ensure polarization even in mildly compromised backgrounds. Here, we have identified a gene regulatory pathway that adds a level of control over cell polarity: regulation of PAR-5 protein levels by alternative 3′ UTR selection. The capacity to tightly regulate PAR-5 expression and adjust *par-5* isoform selection in response to polarity defects confers robustness to the polarity establishment system.

EXPERIMENTAL PROCEDURES

Worm Strains and Maintenance

C. elegans strains were maintained at 16°C or 20°C (fluorescent lines) on NGM (nematode growth media) with *E. coli* OP50 as a food source. Transgenic *par-5* lines were generated by Mos1-mediated single-copy insertion (Frøkjaer-Jensen et al., 2008) into *ttTi5605* on chromosome II (strains EG4322 and EG6699). Full-length, single-copy integration was confirmed by PCR. Strain genotypes can be found in Table S3. Expression of ectopic PAR-5 and GFP::PAR-5 resembled endogenous *par-5* expression because (1) it could complement the *par-5(it55)* mutant, (2) isoform selection was comparable to endogenous *par-5* (Figure S3D), and (3) both loci gave rise to similar protein levels (Figure S6A).

RNAi-Mediated Depletion

Gene knockdown by feeding double-stranded RNA (dsRNA) was performed essentially as described previously by Kamath et al. (2001) and Timmons and Fire (1998). L4 worms were transferred to an RNAi plate for variable durations depending on the experiment, ranging from 6 to 48 hr (Table S4). Worms on RNAi plates were kept at 25°C, except when temperature-sensitive strains were tested, in which case, strains were kept at 16°C. The strength of RNAi was modulated by adjusting the time the worms were kept on the RNAi plate or by dilution with bacteria containing the empty L4440 vector. For the control conditions, bacteria containing either the empty vector or an mCherry RNAi feeding construct were used.

Embryonic Lethality Test

Embryonic lethality was scored by transferring at least ten gravid hermaphrodites to an NGM-OP50 plate for 1 hr (at 25°C) or 2 hr (at 16°C), at which time the mothers were removed and the laid eggs counted. After 2 days and 4 days, respectively, the number of hatched worms was counted.

RNA Isolation and cDNA Synthesis

A total of 20–100 adult worms (more in the case of early larval stages) or isolated eggs or gonads were collected in 0.1 M NaCl, and mRNA was isolated using the TRIzol reagent (Life Technologies) according to the manufacturer's protocol. cDNA for qPCR experiments was generated using oligo-dT primer and M-MuLV reverse transcriptase (Thermo Scientific) according to the manufacturer's protocol.

3′ RACE

For the detection of mRNA isoform 3′ ends, reverse transcription was performed using an oligo(dT) primer containing an additional random unique sequence ("anchor": 5′-GCATTAAATGCGACTCAGG-3′). PCR was performed with the anchor primer and a gene-specific primer using High Fidelity PCR Enzyme Mix (Thermo Scientific) according to the manufacturer's protocol.

qPCR

For qPCR, one or two primer pairs per transcript were designed to span (if possible) an exon-exon junction in order to exclude a contribution from genomic DNA or unspliced pre-mRNA (Table S5). Amplification and detection were performed in triplicate using iQ SYBR Green Supermix (Bio-Rad) on an iQ5 Real-Time PCR Detection System (Bio-Rad) as a two-step PCR (10 s at 95°C and 30 s at 60°C). Nontemplate controls were included, and a melting curve was generated to confirm the amplification of the expected product. Primers were tested with serial dilutions of cDNA for efficiency and quantitativeness.

mRNA fold changes between two conditions were calculated using the -ΔΔCt method (Livak and Schmittgen, 2001). As calibrator gene, *ctb-1*, *spd-2*, or *mex-5* was used, depending on the experiment. For the quantification of transcript abundance, mRNA levels of the target gene were normalized to a control gene (*ctb-1* or *mex-5*). For the quantification of contributions of *par-5* mRNA isoforms to total *par-5* mRNA, isoform levels for *par-5::utr.1* and *par-5::utr.2* were normalized to total *par-5* mRNA levels as determined using primers binding in the common coding sequence. Because *par-5::utr.3* does not have any unique sequence or junction, it could not be detected directly, but its abundance was inferred by subtracting *par-5::utr.1* and *par-5::utr.2* from total *par-5* mRNA levels.

par-5 mRNA in the gonad makes up most of total *par-5* mRNA in the worm because mRNA isolation from worms lacking a germline (*pgl-1(bn101)*) only yielded 20% of *par-5* mRNA present in whole wild-type worms. Conversely, mRNA isolated from gonads was strongly enriched in *par-5* mRNA compared to whole worms. Isoform ratios in whole worms therefore are a good approximation of the situation in the gonad and are not subject to the technical difficulties and consequent variability of mRNA isolation specifically from gonads.

mRNA Sequencing

Detailed information on deep sequencing and data analysis can be found in the Supplemental Experimental Procedures.

Immunofluorescence Protein Localization

Immunofluorescence was performed essentially as described by Oegema et al. (2001). Samples on poly-L-lysine-coated glass slides were fixed in −20°C methanol for 15 min. Primary (rabbit α-PAR-2 [1:300; gift from Carsten Hoege, MPI-CBG; Hoege et al., 2010] or mouse α-PAR-3 [1:600; Developmental Studies Hybridoma Bank]) and secondary (α-rabbit-Alexa 488 [1:500; Molecular Probes] or α-mouse-Alexa 564 [1:500; Molecular Probes]) antibody was added in PBS plus 0.5% Triton X-100 plus 2% BSA, and DNA was visualized using 10 μg/ml DAPI.

Images were acquired on a DeltaVision (Applied Precision) wide-field inverted Olympus IX71 microscope equipped with a CCD camera and a Xenon lamp using a 60× 1.4 NA Plan Apochromat objective, controlled by SoftWorx. Exposure times varied according to staining efficiency and signal intensity from 50 to 800 ms. For each experiment, acquisition conditions were kept constant. The boundary between cortical PAR domains was determined based on the extent of the PAR-3 domain because the reduction in PAR-2 levels in *par-2(or640)* embryos precluded direct measurement of PAR-2 domain size.

Live-Cell Imaging

Embryos for live-cell imaging were prepared as described (Bossinger and Cowan, 2012). Imaging was usually done on a DeltaVision wide-field inverted Olympus IX71 microscope equipped with a CCD camera and a Xenon lamp using a 60× 1.4 NA Plan Apochromat objective, controlled by SoftWorx. Usually, a single midplane image was acquired using the following settings:

- GFP::PAR-2 and GFP::PAR-5: excitation 490/20 nm, emission 528/38 nm; exposure time: 1 s (PAR-2) or 400 ms (PAR-5); neutral density filter: 50%, 1× binning; and
- mCherry::PAR-6 and mCherry::PAR-2: excitation 555/28 nm, emission 617/73 nm; exposure time: 1 s; neutral density filter: 50%, 1× binning.

For display, images were deconvolved using SoftWorx.

Although fluorescence intensity measurements were generally done on a DeltaVision wide-field microscope, results were confirmed on a Zeiss laser-scanning microscope. Images were taken either on an LSM 510 Zeiss microscope using a 63× 1.4 NA Plan Apochromat objective with a diode laser at 488 nm at 2% laser power, a completely open pinhole, and a pixel size of 0.14 × 0.14 μm, or on an LSM 780 Zeiss microscope using a 63× 1.4 NA Plan Apochromat objective with an argon laser at 488 nm at 1% laser power. For embryos, five Z slices were acquired with 3 μm spacing.

Image Analysis

GFP::PAR-5 fluorescence intensity was calculated from DeltaVision or confocal images by selecting and analyzing a region containing the embryo using ImageJ. Average background intensity measured in a region outside the embryo was subtracted from the average intensity in the embryo region. The integrated intensity of the embryo was determined by multiplying the size of the region containing the embryo with its background-subtracted average intensity.

At given time points, measurement of PAR-2 domain size was carried out by manually measuring the extent of the cortical area enriched in fluorescently labeled PAR-2 at NEBD relative to the circumference of the embryo (in ImageJ). For time course analysis, a 20 pixel-wide line along the cortex from the posterior to the anterior pole was selected, and the maximal fluorescence intensities along this line for each time point were measured (ImageJ). Domain sizes were then determined using GNU Octave v.3.2.3 by standardizing embryo length, calculating a running average, subtracting the minimal value, and identifying the position at which the running average drops below the half-maximal value. The mean value of multiple embryos was calculated for each time point, standardized to NEBD.

Cortical accumulation of GFP::PAR-2 from symmetry breaking to NEBD was determined by calculating—for each time point—the ratio of the mean of the maximal intensities of three nonoverlapping cortical regions around the posterior pole to the mean of the average intensities of three nonoverlapping cytoplasmic regions close to the anterior pole (ImageJ). Regions were approximately 3 μm^2.

Contribution of *par-5* Isoforms to PAR-5 Protein

The contribution of individual mRNA isoforms to PAR-5 protein levels was determined using GFP::PAR-5 fusion constructs under the control of wild-type or isoform-specific *par-5* 3′ UTRs. Production of only the isoform(s) indicated was confirmed by 3′ RACE using a gfp-specific primer. All PCR products were sequence verified. For an estimation of the relative abundances of isoforms made from *utr.wt*, *utr.1/2*, or *utr.1/3*, gfp-containing transcripts were preamplified by 3′ RACE (15 PCR cycles) and then used for qPCR. In all cases, relative isoform abundances were comparable to endogenous *par-5* (Figure S3D; data not shown). In addition, the isoform specificity of the transgenes was confirmed using selective depletion of *utr.1*- and *utr.2*-containing transcripts (Figure S3E).

Although *par-5::utr.1* is translated when it is the only isoform that can be made, RNAi using dsRNA targeting *par-5::utr.1* and *par-5::utr.2* in a strain expressing GFP::PAR-5 under the control of *par-5::utr.1/3* did not reduce GFP::PAR-5 levels in one-cell embryos, suggesting that *par-5::utr.1* does not contribute to PAR-5 protein in early embryos. This may reflect an absence of *par-5::utr.1* mRNA at this developmental stage. In wild-type *par-5*, the proximal polyadenylation site can be removed by splicing (giving rise to *utr.2*), but if splicing does not occur, the proximal poly(A) site is predominantly used (giving rise to *utr.3*) and rarely, if ever, skipped to use the distal polyadenylation site (giving rise to *utr.1*). The *par-5::utr.1* detected by qPCR might constitute a contribution from tissues other than the gonad. Some *par-5::utr.1* might be present and translated in oocytes and embryos, but this contribution appears to be below our detection limits.

Visualization and Statistical Analysis

Data analysis was performed in GraphPad Prism v.5.0b and GNU Octave v.3.2.3. Statistical analysis was done in GraphPad Prism and R v.2.15.1. GraphPad Prism and GNUPLOT v.4.2/AquaTerm v.1.0.1 were used for data visualization.

ACCESSION NUMBERS

The data have been deposited in the National Center for Biotechnology Information's Gene Expression Omnibus under accession number GSE59705.

SUPPLEMENTAL INFORMATION

Supplemental Information includes Supplemental Experimental Procedures, seven figures, five tables, and four movies and can be found with this article online at http://dx.doi.org/10.1016/j.celrep.2014.08.004.

ACKNOWLEDGMENTS

The authors thank Carsten Hoege, Anthony A. Hyman, Christian Eckmann (MPI-CBG), Nate Goehring (Cancer Research UK, London), and Geraldine Seydoux (Johns Hopkins University, Baltimore) for reagents; Juergen Knoblich, Javier Martinez, and Luisa Cochella for discussion and suggestions at various stages of the project; and Bartlomiej Gebarski and Harue Wada for technical assistance. Solexa sequencing was performed at the CSF NGS Unit (http://www.csf.ac.at). Some worm strains used in this study were provided by the Caenorhabditis Genetics Center, which is funded by the NIH. Research at the IMP is partially funded by Boehringer Ingelheim.

Received: March 13, 2014
Revised: June 24, 2014
Accepted: August 3, 2014
Published: September 4, 2014

REFERENCES

Aristizábal-Corrales, D., Fontrodona, L., Porta-de-la-Riva, M., Guerra-Moreno, A., Cerón, J., and Schwartz, S., Jr. (2012). The 14-3-3 gene par-5 is

required for germline development and DNA damage response in *Caenorhabditis elegans*. J. Cell Sci. *125*, 1716–1726.

Beatty, A., Morton, D., and Kemphues, K. (2010). The *C. elegans* homolog of *Drosophila* Lethal giant larvae functions redundantly with PAR-2 to maintain polarity in the early embryo. Development *137*, 3995–4004.

Beatty, A., Morton, D.G., and Kemphues, K. (2013). PAR-2, LGL-1 and the CDC-42 GAP CHIN-1 act in distinct pathways to maintain polarity in the *C. elegans* embryo. Development *140*, 2005–2014.

Benton, R., and St Johnston, D. (2003). *Drosophila* PAR-1 and 14-3-3 inhibit Bazooka/PAR-3 to establish complementary cortical domains in polarized cells. Cell *115*, 691–704.

Bossinger, O., and Cowan, C.R. (2012). Methods in cell biology: analysis of cell polarity in *C. elegans* embryos. Methods Cell Biol. *107*, 207–238.

Decker, M., Jaensch, S., Pozniakovsky, A., Zinke, A., O'Connell, K.F., Zachariae, W., Myers, E., and Hyman, A.A. (2011). Limiting amounts of centrosome material set centrosome size in *C. elegans* embryos. Curr. Biol. *21*, 1259–1267.

Fievet, B.T., Rodriguez, J., Naganathan, S., Lee, C., Zeiser, E., Ishidate, T., Shirayama, M., Grill, S., and Ahringer, J. (2013). Systematic genetic interaction screens uncover cell polarity regulators and functional redundancy. Nat. Cell Biol. *15*, 103–112.

Frøkjaer-Jensen, C., Davis, M.W., Hopkins, C.E., Newman, B.J., Thummel, J.M., Olesen, S.P., Grunnet, M., and Jorgensen, E.M. (2008). Single-copy insertion of transgenes in *Caenorhabditis elegans*. Nat. Genet. *40*, 1375–1383.

Goehring, N.W., and Hyman, A.A. (2012). Organelle growth control through limiting pools of cytoplasmic components. Curr. Biol. *22*, R330–R339.

Goehring, N.W., Trong, P.K., Bois, J.S., Chowdhury, D., Nicola, E.M., Hyman, A.A., and Grill, S.W. (2011). Polarization of PAR proteins by advective triggering of a pattern-forming system. Science *334*, 1137–1141.

Greenan, G., Brangwynne, C.P., Jaensch, S., Gharakhani, J., Jülicher, F., and Hyman, A.A. (2010). Centrosome size sets mitotic spindle length in *Caenorhabditis elegans* embryos. Curr. Biol. *20*, 353–358.

Hoege, C., Constantinescu, A.T., Schwager, A., Goehring, N.W., Kumar, P., and Hyman, A.A. (2010). LGL can partition the cortex of one-cell *Caenorhabditis elegans* embryos into two domains. Curr. Biol. *20*, 1296–1303.

Kamath, R.S., Martinez-Campos, M., Zipperlen, P., Fraser, A.G., and Ahringer, J. (2001). Effectiveness of specific RNA-mediated interference through ingested double-stranded RNA in *Caenorhabditis elegans*. Genome Biol *2*, RESEARCH0002.

Kemphues, K.J., Priess, J.R., Morton, D.G., and Cheng, N.S. (1988). Identification of genes required for cytoplasmic localization in early *C. elegans* embryos. Cell *52*, 311–320.

Kuroyanagi, H., Kimura, T., Wada, K., Hisamoto, N., Matsumoto, K., and Hagiwara, M. (2000). SPK-1, a *C. elegans* SR protein kinase homologue, is essential for embryogenesis and required for germline development. Mech. Dev. *99*, 51–64.

Labbé, J.C., Pacquelet, A., Marty, T., and Gotta, M. (2006). A genomewide screen for suppressors of par-2 uncovers potential regulators of PAR protein-dependent cell polarity in *Caenorhabditis elegans*. Genetics *174*, 285–295.

Livak, K.J., and Schmittgen, T.D. (2001). Analysis of relative gene expression data using real-time quantitative PCR and the 2(-Delta Delta C(T)) method. Methods *25*, 402–408.

Mangone, M., Manoharan, A.P., Thierry-Mieg, D., Thierry-Mieg, J., Han, T., Mackowiak, S.D., Mis, E., Zegar, C., Gutwein, M.R., Khivansara, V., et al. (2010). The landscape of *C. elegans* 3'UTRs. Science *329*, 432–435.

Martin, D., Brown-Luedi, M., and Chiquet-Ehrismann, R. (2003). Tenascin-C signaling through induction of 14-3-3 tau. J. Cell Biol. *160*, 171–175.

Merritt, C., Rasoloson, D., Ko, D., and Seydoux, G. (2008). 3′ UTRs are the primary regulators of gene expression in the *C. elegans* germline. Curr. Biol. *18*, 1476–1482.

Morton, D.G., Shakes, D.C., Nugent, S., Dichoso, D., Wang, W., Golden, A., and Kemphues, K.J. (2002). The *Caenorhabditis elegans* par-5 gene encodes a 14-3-3 protein required for cellular asymmetry in the early embryo. Dev. Biol. *241*, 47–58.

Morton, D.G., Hoose, W.A., and Kemphues, K.J. (2012). A genome-wide RNAi screen for enhancers of par mutants reveals new contributors to early embryonic polarity in *Caenorhabditis elegans*. Genetics *192*, 929–942.

Motegi, F., and Seydoux, G. (2013). The PAR network: redundancy and robustness in a symmetry-breaking system. Philos. Trans. R. Soc. Lond. B Biol. Sci. *368*, 20130010.

Motegi, F., Zonies, S., Hao, Y., Cuenca, A.A., Griffin, E., and Seydoux, G. (2011). Microtubules induce self-organization of polarized PAR domains in *Caenorhabditis elegans* zygotes. Nat. Cell Biol. *13*, 1361–1367.

Munro, E., Nance, J., and Priess, J.R. (2004). Cortical flows powered by asymmetrical contraction transport PAR proteins to establish and maintain anterior-posterior polarity in the early *C. elegans* embryo. Dev. Cell *7*, 413–424.

Nakanishi, K., Hashizume, S., Kato, M., Honjoh, T., Setoguchi, Y., and Yasumoto, K. (1997). Elevated expression levels of the 14-3-3 family of proteins in lung cancer tissues. Hum. Antibodies *8*, 189–194.

Oegema, K., Desai, A., Rybina, S., Kirkham, M., and Hyman, A.A. (2001). Functional analysis of kinetochore assembly in *Caenorhabditis elegans*. J. Cell Biol. *153*, 1209–1226.

Pacquelet, A., Zanin, E., Ashiono, C., and Gotta, M. (2008). PAR-6 levels are regulated by NOS-3 in a CUL-2 dependent manner in *Caenorhabditis elegans*. Dev. Biol. *319*, 267–272.

Perathoner, A., Pirkebner, D., Brandacher, G., Spizzo, G., Stadlmann, S., Obrist, P., Margreiter, R., and Amberger, A. (2005). 14-3-3sigma expression is an independent prognostic parameter for poor survival in colorectal carcinoma patients. Clin. Cancer Res. *11*, 3274–3279.

Porter, G.W., Khuri, F.R., and Fu, H. (2006). Dynamic 14-3-3/client protein interactions integrate survival and apoptotic pathways. Semin. Cancer Biol. *16*, 193–202.

Sönnichsen, B., Koski, L.B., Walsh, A., Marschall, P., Neumann, B., Brehm, M., Alleaume, A.M., Artelt, J., Bettencourt, P., Cassin, E., et al. (2005). Full-genome RNAi profiling of early embryogenesis in *Caenorhabditis elegans*. Nature *434*, 462–469.

Takihara, Y., Matsuda, Y., and Hara, J. (2000). Role of the beta isoform of 14-3-3 proteins in cellular proliferation and oncogenic transformation. Carcinogenesis *21*, 2073–2077.

Timmons, L., and Fire, A. (1998). Specific interference by ingested dsRNA. Nature *395*, 854.

Tzivion, G., Gupta, V.S., Kaplun, L., and Balan, V. (2006). 14-3-3 proteins as potential oncogenes. Semin. Cancer Biol. *16*, 203–213.

Venables, J.P., Tazi, J., and Juge, F. (2012). Regulated functional alternative splicing in *Drosophila*. Nucleic Acids Res. *40*, 1–10.

Waddington, C.H. (1942). Canalization of development and the inheritance of acquired characters. Nature *150*, 563–565.

Wang, W., and Shakes, D.C. (1997). Expression patterns and transcript processing of ftt-1 and ftt-2, two *C. elegans* 14-3-3 homologues. J. Mol. Biol. *268*, 619–630.

Zonies, S., Motegi, F., Hao, Y., and Seydoux, G. (2010). Symmetry breaking and polarization of the *C. elegans* zygote by the polarity protein PAR-2. Development *137*, 1669–1677.